Journal of
Ceramic Science
and Technology

J. Ceram. Sci. Tech., **04** [01] 11-18 (2013)
DOI: 10.4416/JCST2012-00033
available online at: http://www.ceramic-science.com

Submicrometer Silica Spheres Generated by Laser Fuming

C.M. Gomes[1], R. Müller[1], J. Günster[*1], T. Mühler[2], R. Görke[2], J.G. Heinrich[2]

[1]BAM Federal Institute of Materials Research and Testing, Unter den Eichen 87, 12205 Berlin, Germany
[2]Clausthal University of Technology, Institute of Nonmetallic Materials,
Zehntnerstr. 2a, 38678 Clausthal-Zellerfeld, Germany

received September 19, 2012; received in revised form January 15, 2013; accepted January 30, 2013

Abstract

The production of agglomerate-free SiO_2 particles exhibiting a monomodal distribution of particle sizes of around 300 nm by means of direct laser fuming of micrometric SiO_2 powders has been successfully demonstrated. With a 12 kW cw CO_2 laser system, a production rate of up to 1 kilogram powder per hour was achieved. Almost ideal spherical amorphous SiO_2 particles in a broad particle size distribution between 10 nm and several 100 nm ($d_{50} \approx 300$ nm) were synthesized. Several observations suggest weak agglomeration forces between the particles. A temperature reduction of 200 °C for sintering powder compacts was observed.

Keywords: Laser, SiO_2, nanopowder

I. Introduction

One of the main advantages of using submicrometer powders for the fabrication of ceramic parts relies on the considerable reduction of the required sintering temperature. Consequently, different technologies have been developed in recent years in order to achieve ever finer particle sizes. Among the most common routes, the chemical methods, such as nucleation and growth, hydrolysis of salt solutions, sol-gel, gas-phase reaction as well as the newly developed "gel combustion" [1] have become well established both commercially and technically [2]. On the other hand, the mechanical routes, based on particle size reduction with grinding of coarse powders, have also evolved thanks to the latest developments in energy milling methods [3]. Among the thermal routes, flame spray pyrolysis (FSP) has been established as one of the most common methods applied for the synthesis and large-scale production of ceramic powders in submicrometer and nano-scale sizes [4, 5, 6]. With the adjustment of certain process parameters, it has been possible to produce ceramic nano-particles from different systems like, for instance, zinc oxide [7 8], alumina [9], magnesium-aluminate [10], titania [11] and zirconia [4]. However, control of the powder morphology as well as the particle size distribution is sometimes limited. Another issue is related to the achievement of particle sizes in the range of 5 nm but only in form of 100 nm agglomerated structures, which are undesirable for the further steps in ceramic processes, i.e. forming and sintering. The generation of ceramic nano-particles based on direct laser-gas reaction has also been reported [12]. In another approach, CO_2 lasers are coupled into flame spray pyrolysis [13]. With this method, the powder was irradiated just after leaving the spraying nozzle. The irradiated aggregates were heated to high temperatures, to be sintered afterwards to more sphere-like particles.

In general, laser technologies are well established for processing all classes of materials. Laser systems can provide energy in a defined volume in a controlled process. Furthermore, the transfer of process heat by means of lasers does not involve the risk of contamination or chemical reactions with gaseous media from, for example, a combustion process. Besides the fact that a variety of laser technologies have already found their way into industrial application, these unique properties are continuously stimulating new applications for lasers as energy sources in thermal processing. Besides laser machining technologies for ceramics like cutting, drilling, welding and polishing [14], the evaporation or ablation of ceramic materials for the generation of nano-disperse ceramic particles has evolved to an active field of research:

Laser vaporization has been seen as a promising novel nano-particle synthesis route based on laser heating of raw materials by direct irradiation of a target with a laser beam. According to Sysoev *et al.* [15], different processes can take place at the target depending on the applied laser power density (Ps). On the irradiation of silica glass rods with a CO_2 laser beam, it was possible to observe heating without plastic deformation ($Ps < 0.5$ kW/cm^2), material melting ($0.5 < Ps < 1$ kW/cm^2), material melting with vaporization ($1 < Ps < 10$ kW/cm^2) or high-rate sublimation ($Ps > 10$ kW/cm^2).

Laser ablation is described in the literature as a process for removing macroscopic amounts of material, in a non-equilibrium thermodynamic state. The process is often characterized by the formation of a plume of ionized specimens. Here, the vaporization rate as well as the products of vaporization also strongly depend on the laser power density (Ps), which in turn depends on the relative posi-

* Corresponding author: jens.guenster@bam.de

tion of the focal plane to the surface of the irradiated material [16, 17, 18]. With laser ablation of a ceramic bulk or a powder bed, by means of a focused laser beam, the production of ZrO_2 nano-particles was demonstrated in [16]. Depending on the applied laser power (1 – 4 kW), up to 130 g of ZrO_2 per hour has been produced. In addition to the laser power density, the dimension of the irradiated area was also found to be a factor influencing the surface area of the obtained particles. [17 and 18] report on the production of nano-particles from Al_2O_3, ZrO_2 and TiO_2, both from a single component as well as from stoichiometric mixtures of these oxides. The laser configuration consisted of a focused 2 kW CO_2 laser beam operating in continuous mode.

Laser fuming is performed at moderate laser power densities, normally in the range of 1 kW/cm^2, significantly below the ablation threshold for ceramic materials. In this case, a thermodynamic equilibrium can be established and the energy of the impinging laser can dissipate into heat without ionization of the specimens. With the use of a CO_2 laser system, SiO_2 can be annealed easily, as most of the impinging laser light (wavelength 10.6 μm) is dissipated into heat by direct photon-phonon interaction. At 10-μm wavelengths, the diffractive index of SiO_2 is about 2, amounting to approximately 10 % reflected intensity at normal incidence of the light [19]. As a consequence of the laser-induced heat generation, the vaporization of molecular silicon oxide species from the surface of a melt pool takes place. According to [20, 21, 22], decomposition of SiO_2 at high temperatures is mediated by the formation of silicon monoxide (SiO) according to Eq. (1):

$$2SiO_{2\ (liquid)} \rightarrow 2SiO_{(gaseous)} + O_2 \qquad (1)$$

The atmosphere just above the hot spot in the melt pool provides a large temperature gradient for the evaporated material. Hence, the evaporated silicon oxide forms a supersaturated vapor phase above the hot spot, the condensation to a fume of silica particles can be observed even with the naked eye. Since the formation of the fumed silica submicrometer particles is in a thermodynamic equilibrium process, the authors named this type of vaporization process laser fuming.

In Snytnikov *et al.* [23] the production of submicrometer Al_2O_3 and ZrO_2 particles by means of laser fuming from ceramic powder has been demonstrated. With a continuous CO_2 laser (≤ 120 W), up to 1 g powder per hour has been produced. Noticeable was the amorphous character of the generated powders. The production of small amounts of stoichiometric nano-sized borosilicate glass powders from glass rods has been reported by Clasen [20]. These particles could be fully sintered to a transparent glass at 800 °C.

Several potential advantages make *laser fuming* a unique technique within the variety of laser vaporization processes. Just to mention some of these, owing to the formation of a macroscopic pool of several cm^3 of molten material and effective mixing of the melt pool via convection-induced mass flow, the described laser fuming process can be applied to material powder blends without selective vaporization of the single powder specimen (Fig. 1). Secondly, owing to the high temperature gradient established above the melt pool, ceramic powders with a unique phase composition might be achieved thanks to the quenching of the condensed particles. The high cooling rate during particle condensation favours the formation of amorphous particles above crystalline ones. Finally, since vaporization starts after complete intermixing of the raw materials within the melt, a continuous self-re-feed and contamination-free melt pool is achieved, which is expected to allow the production of submicrometer and nano particles from a mixture of oxides with, for example, a final eutectic composition.

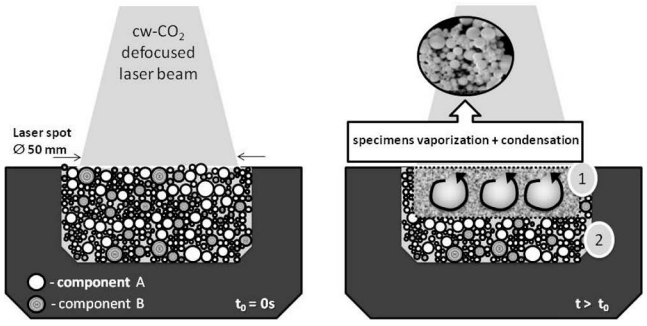

Fig. 1: Schematic laser fuming process of SiO_2 powder. (1) Melt pool and heat-affected area: the heat is transferred from the laser-affected upper side of the melt to the bottom through convection and heat and light conduction. (2) Region containing the unmolten ceramic particles: self re-feed of the melt pool.

A CO_2 laser system, providing a power output up to 12 kW in continuous wave (cw) mode, was combined with a defocused optical system. As a result, the primary laser beam could be widened to a spot size of 100 mm and the formation of a macroscopic melt pool of some cm^3 in volume could be attained. The purpose of this paper is to present the first results for the production of submicrometer SiO_2 particles by means of laser fuming with a defocused CO_2 laser system. From micrometric high-purity silica as the raw material, agglomerate-free SiO_2 particles have been produced. The powders formed have been characterized by means of imaging analysis techniques and their sintering activity has been described.

II. Experimental Procedure

For the laser vaporization experiments, a commercially available ultra-pure amorphous silica powder, purchased from Mitsubishi Co. Japan, with a d_{50} of 100 μm and metal impurities totalling less than 300 ppb was used.

During laser treatment, the silica powder was placed in a 500-cm^3 cylindrical graphite crucible measuring 100 mm in diameter and positioned in the beam line of a CO_2 laser system (TLF 12000 turbo, TRUMPF, Germany) providing a power output of up to 12 kW continuous wave (cw). The CO_2 laser light, emitting at a wavelength of 10.6 μm, is readily absorbed by most ceramic materials. The linear polarized primary laser beam, 25 mm in diameter, was shaped by a single concave mirror lens with a focal length of f = 300 mm. The sample was placed relative to the optics in a way that a circular laser spot of 50 mm in diameter was generated on the sample surface. The central laser beam impinges with normal incidence onto the horizontally oriented sample surface. With the given parameters, a maximum mean incident laser power density (Ps) of

611 W/cm^2 is calculated on the sample surface, however, inhomogeneities in the beam profile result in local power densities of up to 50 % higher than the mean value.

The condensed fume was extracted from the hot sample surface via a vacuum extraction system operating with conventional dry filters. The filters are not optimized for the collection of nano-sized particles and it is likely that they discriminate smallest particles such that they are not collected with the same rate as larger particles. On the other hand, after the collection of a significant amount of particles subsequent clogging of the filter improves its ability to collect silica particles of all sizes, even the smallest particles. The analysis of the collected particles was performed under this premise.

Obtained particles were characterized by means of electron microscopy (FEI Helios Nanolab 600). Particle size and particle size distribution were measured with an ultra sound spectrometer (DT 1200, Quantachrome, Germany). The measurements were performed in water media with stabilization of the powder by the addition of NaOH until a pH of 8.3 was reached.

The sintering behaviour was studied on 5 x 5 x 5 mm powder compacts prepared by means of uniaxial pressing. The volumetric shrinkage was measured with a heating microscope (EM-201, Hesse Inst., Germany), at a heating rate of 10 °C/min, up to 1400 °C. The projected image of the sample during sintering was measured with a camera system. The images were collected at a rate of 40 frames per minute.

III. Results

Fig. 2 shows the pool of melted quartz glass formed during the laser fuming of the high-purity amorphous silica studied. As shown previously [24], a mean laser power density of about 150 W/cm^2 was sufficient to reach temperatures exceeding the softening point of amorphous silica, 1713 °C [25]. At this power density, the silica powder started to melt almost instantaneously upon laser exposure. This good annealing efficiency is reported to be derived from the high absorbance of the CO_2 laser radiation in silica glass [15]. Accordingly, the energy provided by the laser light dissipates into heat at the silica sample's surface. Owing to thermal conduction within the silica powder, prolonged laser treatment results in the formation of a pool of molten silica of several cm^3 in volume, which is supported by the not yet molten silica powder, ensuring that no crucible material can contaminate the silica melt.

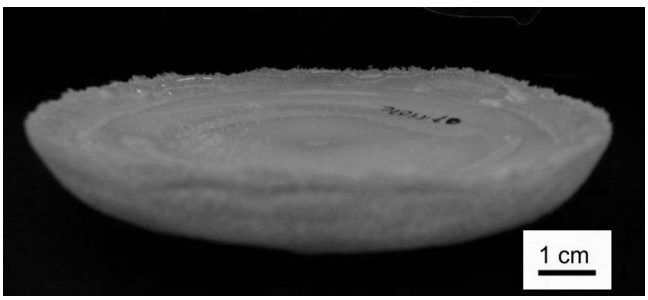

Fig. 2: Pool of molten quartz glass formed during the laser fuming of high-purity amorphous silica after cooling down to room temperature.

Excessive vaporization of SiO_2 from the melt pool formed in this way could be observed at mean power densities > 150 W/cm^2. This phenomenon could be easily recognized by the formation of a white fume over the melt pool. The fume must have been formed by the vaporization process directly from the overheated silica melt since the applied power density (Ps) was far below the ablation threshold of silica. Nonetheless, the laser-irradiated surface should have reached a significantly high temperature, promoting the detachment of silicon oxide specimens from the liquid to the vapour phase as suggested in [21] and [26]. This viewpoint is supported by the observation that no boiling of the silica melt in the pool was evidenced, even at the highest vaporization rates.

During the continuous emission of material via vaporization, the melt pool did not change significantly in volume. Material from the silica powder bed continuously replaced the lost material.

By means of the discussed setup, vaporization rates exceeding 1 kg per hour could be reached. Given an electrical energy efficiency of the CO_2 laser system of typically 10 %, an energy consumption of approximately 120 kWh could be estimated for the production of 1 kg powder. This would correspond to energy costs of approx. 10 US$ per 1 kg of nano particles. Taking into account five years equipment depreciation and a capital expenditure of 600 000 US$ for the described laser system, an additional cost of approx. 13 US$ per kg powder should be considered.

In Fig. 3, a representative micrograph of the produced silica powder is shown. The powder consists of almost ideally spherical beads of submicrometer size. Since no crystalline phase could be detected with XRD (not shown), the obtained particles can be regarded as amorphous silica. Most striking, however, since this is highly appreciated for ceramic processing of submicrometer powders, the

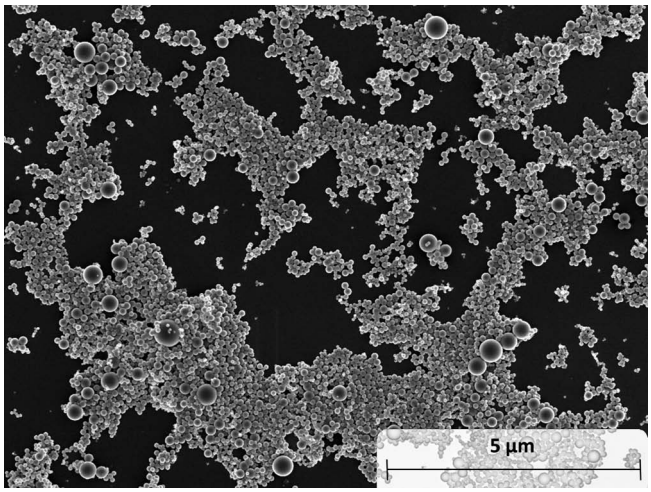

Fig. 3: Quartz glass beads formed by laser fuming of high-purity amorphous silica.

particle alignment seen in Fig. 3 clearly suggests weak agglomeration forces. Thus, the small particles, which have been condensed from water steam onto the substrate, are arranged closely packed almost in mono-layers. Large spheres stand out of these mono-layers, but they are almost free of agglomerated smaller ones. Additionally,

there is no hint of large three-dimensional agglomerates formed before particle deposition onto the substrate.

Fig. 4 shows the mean particle size and particle size distribution of the fumed SiO_2 particles. A d_{50} of 300 nm was measured in a water-based suspension containing the powder. At pH 8.3, values for the zeta potential at the surface of the particles were found to be between 41 and 43 mV. This size distribution was confirmed with image analysis of the micrographs, which showed particle diameters between 10 nm and some 100 nm.

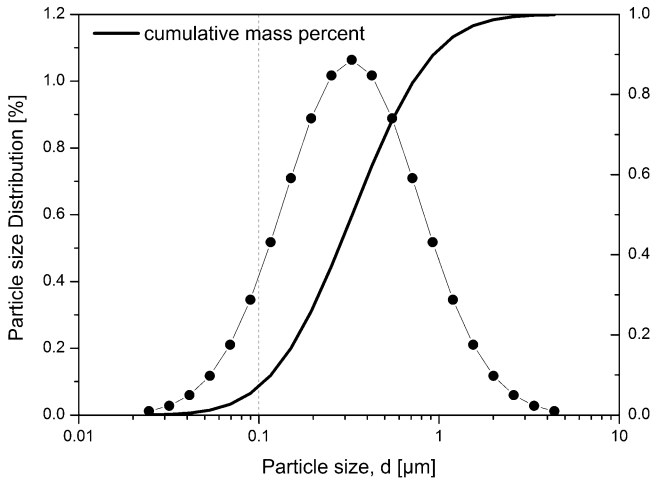

Fig. 4: Particle size and particle size distribution of the fumed SiO_2 nano particles.

This size distribution, however, should depend on process parameters, such as the fume extraction speed out of the laser-influenced volume and the applied laser power density [18]. Both parameters could influence the temperature and super saturation vapour of silicon oxide above the silica melt pool [21, 26]. Furthermore, the nucleation and growth of the liquid silica droplets, which condense into a fume during cooling, should also be considered. Thus, a more rapid extraction of the fume of silica particles, away from the melt pool, would favour the formation of smaller particles and a well-defined extraction speed would make the size distribution narrower.

Fig. 5 presents the sintering curves of compacts prepared from the fumed SiO_2 powder in comparison with a micrometric powder compact ($d_{50} \sim 15$ µm). The latter powder is the raw material used for the laser fuming process, but ground in a jet mill. Thus, the two powders are very similar in respect of their purity. Moreover, their particle surfaces have not been in contact with any material other than the silica powder itself. Owing to some restrictions on the sintering microscope in reaching temperatures higher than 1400 °C, full densification of the samples prepared with the micrometric silica could not be observed. Nonetheless, the final density of the samples prepared with the fumed silica was 2.4 ± 0.2 g/cm^3. This value, aside from being obtained at 1300 °C, is in the density range of quartz glass, 2.2 g/cm^3. In a comparison of the sintering curves, it is clearly noticeable that the onset of shrinkage appears at approximately 200 °C lower temperatures for the laser-fumed powder. This finding is typical for nano powders. Furthermore, however, full densification is reached at a considerably lower temperature as it is indicated by the measured final density. Such behaviour is not always found for nano-scaled materials owing to agglomeration and formation of large residual pores [22]. The rapid final densification of the fumed powders as well as the relatively high powder compact green density of 54 % attained [22] thus indicate weak agglomeration forces.

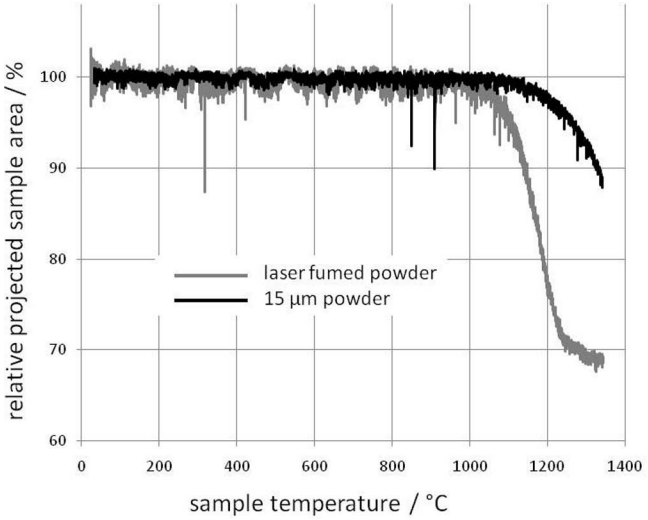

Fig. 5: Sintering curves of the compacts bodies prepared from the nanometric and micrometric powders, respectively. The micrometric powder presented a mean particle size of 15 µm.

IV. Discussion

As a promising key property of the fumed SiO_2 submicrometer particles, weak agglomeration forces were indicated by the observed particle arrangement, the good agreement between particle size distribution data obtained with different methods as well as by a high green density of 54 % concluded from the sintering curve in Fig. 5. However, during the SEM imaging, after a certain time, the particles started to show some evidence of sintering, e.g. neck formation and the reduction of inter-particle porosity.

In order to prove that this effect does not reflect agglomeration during particle formation in the laser fuming process, but is an artefact of the SEM observation, selected samples were exposed to prolonged SEM observation.

During these experiments, a clear change in the morphology of the powders was noticed. Initially loosely packed spherical silica beads turn into agglomerates, based on the formation of sintering necks between adjacent particles, which is characteristic of the initial steps during a sintering process. As an example, Fig. 6 presents a sequence of SEM micrographs taken of an ensemble of silica beads with a broad particle size distribution after different exposition times: line by line from the upper left image to the lower right, the observation time increases in a 240-s succession from 240 s to 960 s, respectively. During this period, the SEM parameters were not changed and the electron beam continuously scanned the imaged area. Taking this into consideration, the particles were continuously exposed to an electron current of 86 pA, with each electron carrying energy of 2000 eV. Electrons with this energy interact very well with the target material as a result of inelastic scattering, and eventually raise the material temperature. With increasing exposure time, the formation of necks between

the particles as well as pore shrinkage becomes clearly noticeable. As a result, differentiation of individual silica particles becomes progressively more difficult. On the other hand, image analysis shows that the distances between the particle centres remain constant. As a final effect, the particle diameters increase slightly. For the most isolated large particle on the left hand (arrow), the diameter increases gradually from approximately 120 nm to 130 nm, equivalent to a volume gain of approx. 8 %.

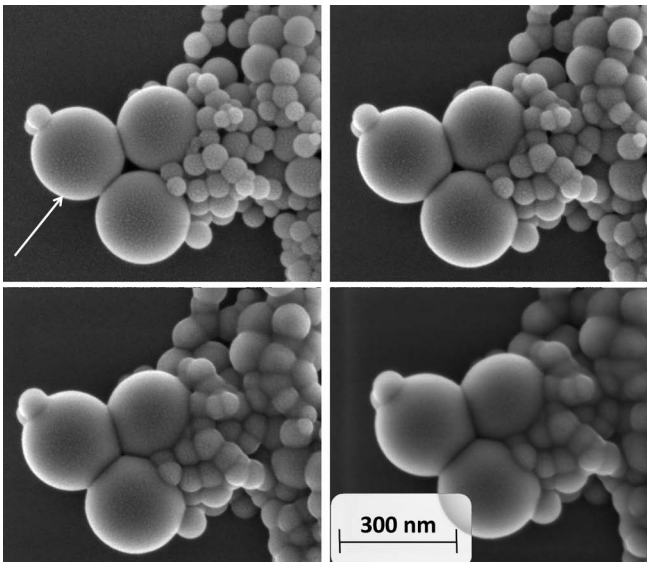

Fig. 6: SEM micrographs of fumed nano SiO_2 beads after different observation times. From upper left to lower right: t = 0 s, 240 s, 480 s, 920 s.

Figs. 7 (a) and (b) shows a chain of interconnected silica beads of similar size after 60 s and 960 s exposure, respectively. Here too, the SEM parameters were not changed and the electron beam continuously scanned the imaged area. It can be observed that the formation of pronounced particle necks is noticeable although the distance between particle centres remains constant. In Fig. 7, however, a more pronounced increase of the size of the imaged particles is evidenced. Thus, the diameter of the largest particle of the cluster increases from ≈ 59 to 82 nm, here again equivalent to a volume gain of circa 40 %.

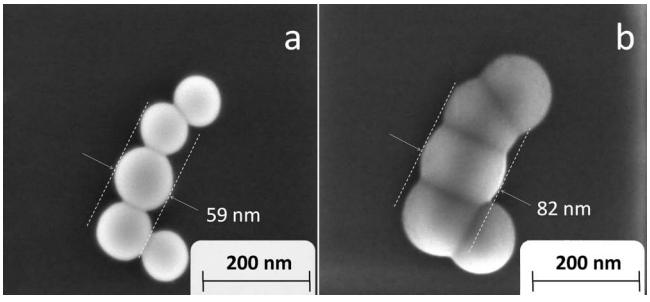

Fig. 7: Quartz glass beads after different exposure times in the SEM. (a) The image was taken after approximately 60 s, in (b) after 960 s. During the analysis, the SEM parameters, especially current (21 pA) and acceleration voltage (2 kV), were not changed.

The observations illustrated in Figs. 6 and 7 might be explained by three different hypotheses:

(1) Upon electron bombardment of the silica, the beads are heated up to temperatures enabling viscous sintering, with flattening of the silica particles affected by gravity and wetting of the substrate.

(2) Upon electron bombardment, the silica beads are heated up to temperatures enabling viscous sintering while simultaneous particle swelling is either pretended by an image error or caused by the electron-beam-induced creation of defects.

(3) Upon electron bombardment, hydrocarbon contamination may be deposited on the silica particles and the substrate. The equilibrium of simultaneous re-vaporization and re-condensation of the carbonaceous species here tends to minimize the specific surface energy, mimicking viscous sintering.

In hypotheses (1) and (2), a considerable *temperature increase* is assumed. During SEM imaging, the imaged object is exposed to an electron beam providing a certain power, which is the product of the acceleration voltage and beam current. When the electron beam is impinging on the imaged object, part of its energy is transferred to the object and dissipated through heat. This process results in an annealing of the imaged object up to an equilibrium temperature at which the energy provided by the electron beam equals the energy lost by heat transfer. Assuming that the thermodynamic equilibrium temperature of the silica beads during SEM imaging is dominated by equilibrating the energy provided by the SEM's electron beam, per unit area of the image and unit time, and the energy loss of the annealed particles by heat radiation according to the Stefan-Boltzmann law, a temperature of the particles up to 2000 °C could be calculated. In this context it is notable that the mean free path of 2 keV electrons in solids is in the range of 10 to 20 nm. In other words, the kinetic energy of 2 keV electrons is almost completely dissipated within the observed particles.

Assuming a viscous sintering mechanism, the ratio of neck to particle diameter, obtained from Fig. 7, also allows rough estimation of the required sintering temperature according to Eq. (2) [27]:

$$\left(\frac{X}{D}\right)^2 = \frac{3\gamma t}{D\eta(T)} \qquad (2)$$

where t, T, X, D, γ, and η represent observation time, temperature, neck radius, particle radius, surface energy, and viscosity of silica glass. Based on Eq. (2) and $\gamma \approx 0.280$ N/m [28], a viscosity in the range log $\eta \approx$ 9.5...9.8 Pa·s would result, which corresponds to temperatures between 1350 and 1400 °C [29].

The assumed *flattening* in hypothesis (1) implies that the volume of the beads may remain constant, while the shape of the beads change in merely their two dimensional projection. Therefore, swelling of the beads under different sample angles together with *"in situ"* preparation of cross-sections of the beads by means of focused ion beam milling was investigated. No significant deformation of the beads was recognized. Hence, no evidence has been found supporting anisotropic deformation of the silica beads in a way that their two-dimensional projection in the SEM images grows when subject to electron bombardment. Furthermore, the effect of *wetting* phenomena does not seem likely since changes in the supporting substrate from metal to glass and carbon had no influence on the observed

swelling and, thus, argues against the suggestion that an interfacial interaction between the silica beads and supporting substrate in a type of wetting drives anisotropic deformation of the beads. Explaining the assumed viscous flattening would finally contradict the viscosity estimated from the observed ratios between neck size and particle diameter. Thus, such viscous flattening would typically require a viscosity below the range of about $\log \eta = 4...5$ Pa·s, which corresponds to the half-sphere point in hot-stage microscopy viscosity measurement techniques [30].

The assumption of *sintering by viscous flow* in hypothesis (1) and (2) cannot be supported by the other results. First of all, the centre distance between all silica particles remains constant. For viscous sintering, such behaviour is difficult to understand. Second, no indications of particle rearrangement and non-homogeneous sintering are seen in Fig. 6, where large particles (left) are glued to a cluster of much smaller particles. Both phenomena are highly expected for viscous sintering. Furthermore, it seems improbable that the observed volume swelling had balanced out the expected linear shrinkage by viscous sintering so that, on balance, the final position of all particles has remained constant.

As part of hypothesis (2), the observed increase in particle size is assumed to be caused by *image errors* owing to charge effects. When the particles were imaged with different acceleration voltages, for instance 2 kV and 20 kV, no evidence to support this hypothesis could be found. Therefore, it is rather doubtful that an increase in the particle area during SEM imaging originates from an imaging error associated with a subsequent charging up of the particles.

As an alternative assumption to hypothesis (2), the increase in particle size is attributed to the swelling of silica particles under the effect of electron bombardment. In the literature a swelling of thin silica layers upon electron bombardment has been reported. Silica grown as native oxide layers on silicon wafers has been treated with 300 keV electron beams [31]. Swelling of graphite as a result of electron bombardment has also been reported by [32]. The increase of lattice constant was attributed to radiation damage of 200 keV electrons saturated at $\Delta C/C \approx 5\times10^{-3}$ at an irradiation dose of 1.5×10^{24} e/m^2 (24 As/cm^2). However, this cannot explain the pronounced size increase observed here, although higher doses of ≈ 50 and 90 As/cm^2 are given. In other studies on the effect of electron radiation on graphite up to 9600 As/cm^2 [33] and photosensitive glasses [34] (11.4 mC/cm^2), no swelling has been reported.

Hypothesis (3) best explains the increase in particle size while the position remains constant. It may also explain the differently pronounced effect in Figs. 6 and 7 owing to different ratios of silica and substrate surface area. Electron-beam-induced contamination of carbonaceous material as assumed in hypothesis (3) is almost always present after viewing in SEM [35, 36]. Vladar [36] reports on several studies in which both the sample itself and the vacuum in the SEM was found to be the material source. Deposition rates up to few tens of nm per second have been reported.

V. Summary

Spherical amorphous submicrometer-sized silica particles have been produced by means of laser fuming. By impinging a defocused CO_2 laser beam onto the surface of a micro-sized SiO_2 powder bed, production rates of approx. 1 kilogram powder per hour could be reached. A reduction of about 200 °C for the sintering temperature of compacts prepared from the produced SiO_2 particles has been observed. In the SEM micrographs, the fumed particles are shown as agglomerate-free powders. On the other hand, sintering necks are formed between adjacent particles after prolonged observation in SEM. Summing up the aspects that could have influenced the SEM observation; it is most likely that electron-beam-induced annealing of the particles together with carbonaceous contamination during SEM observation result in particle agglomeration.

In conclusion, laser fuming seems a promising route for the production of ceramic nano-particles, especially if a mixture of oxides is intended thanks to the "self-re-feed" aspect of the proposed system.

Acknowledgement

Fruitful discussion with M. Bücker and M. Sabel (BAM) is gratefully acknowledged. The authors also wish to thank Mrs Gabriele Steinborn (BAM) for the particle size measurements.

References

1 Deorsola, F.A., Vallauri, D.: Synthesis of TiO_2 nanoparticles through the gel combustion process, *J. Mater. Sci.*, **43**, 3274 – 3278, (2008).

2 Brook, R.J.: Materials science and technology – a comprehensive treatment, from processing of ceramics. Part I, Vol. 17A, VCH, Germany, 1996.

3 Knieke, C., Romeis, S., Peukert, W.: Influence of process parameters on breakage kinetics and grinding limit at the nanoscale, *AIChE J.*, **57**, [7], 1751 – 1758, (2011).

4 Helble, J.J.: Combustion aerosol synthesis of nanoscale ceramic powders, *J. Aerosol Sci.*, **29**, [5 – 6], 721 – 736, (1998).

5 Kammler, H.K, Madler, L., Pratsinis, S.E.: Flame synthesis of nanoparticles, *Chem. Eng. Techn.*, **24**, [6], 583 – 596, (2001).

6 Kammler, H.K., Mueller, R., Senn. O., Pratsinis, S.E.: Synthesis of silica-carbon particles in a turbulent H_2-air frame aerosol reactor, *AIChE Journal*, **47**, [7], 1533 – 1543, (2001).

7 Marshall, B.S., Telford, I., Wood, R.: A field method for the determination of zinc oxide fume in air, *Analyst*, **96**, 569 – 578, (1971).

8 Carroz, J.W.,Odencrantz, F.K., Finnegan, W.G., Drehmel, D.C.: Aerosol generation to simulate specific industrial fine particle effluents, *Am. Ind. Hyg. Assoc. J.*, **41**, [2], 77 – 84, (1980).

9 Sokolowski, M., Sokolowska, A., Michalski, A., Gokieli, B.: The "in-flame-reaction" method for Al_2O_3 aerosol formation, *J. Aerosol Sci.*, **8**, 219 – 229, (1977).

10 Bickmore, C.R., Waldner, K.F., Treadwell, D.R., Laine, R.M.; Ultrafine spinel powders by flame spray pyrolysis of a magnesium aluminum double alkoxide, *J. Am. Ceram. Soc.*, 79, [5], 1419 – 1423, (1996).

11 Bickmore, C.R., Waldner, K.F., Baranwal, R., Hinklin, T., Treadwell, D.R., Laine, R.M.: Ultrafine titania by flame spray pyrolysis of a titanatrane complex, *J. Eur. Ceram. Soc.*, **18**, [4], 287 – 297, (1998).

12 Cannon, W.R., Danforth, S.C., Flint, J.H., Haggerty, J.S., Marra, R.A.: Sinterable ceramic powders from laser-driven reac-

tions: I, Process description and modeling, sinterable ceramic powders from laser-driven reactions: II, Powder characteristics and process variables, *J. Am. Ceram. Soc.*, **65**, [7], 324 – 335, (1982).

13 Lee, D., Choi, M.: Control of size and morphology of nano particles using CO_2 laser during flame synthesis, *J. Aerosol Sci.*, **31**, [10], 1145 – 1163, (2000).

14 Ready, J.F., Farson, D.F., Feeley, T. (Eds.), LAI Handbook of laser material processing, ISBN: 0912035153, Springer-Verlag, 2010.

15 Sysoev, V.K., Masychev, V.I., Papchenko, B.P., Ya Rusanov, S., Yakovlev, A.A., Glukhoedov, N.P.: High-rate IR laser vaporization of silica glass, *Inorg. Mater.*, **39**, [5], 634 – 640, (2003).

16 Michel, G., Mueller, E., Oestreich, C., Staupendahl, G., Henneberg. K.H.: Ultrafine ZrO_2 powder by laser vaporization: preparation and properties, *Mat.-Wiss. u. Werkstofftech.*, **27**, 345 – 349, (1996).

17 Kurland, H.-D., Stoetzel, C., Grabow, J., Zink, I., Mueller, E., Staupendahl, G., Mueller, F.A.: Preparation of spherical titania nanoparticles by CO_2 laser vaporization and process-integrated particle coating, *J. Am. Ceram. Soc.*, **93**, [5], 1282 – 1289, (2010).

18 Kurland, H.-D., Grabow, J., Müller, F.A.: Preparation of ceramic nanospheres by CO_2 laser vaporization (LAVA), *J. Eur. Ceram. Soc.*, **31**, [14], 2559 – 2568, (2011).

19 Günster, J., Heinrich, J.G., Schwertfeger, F.: Laser sintering of ultra pure SiO_2 crucibles, *Int. J. Appl. Ceram. Technol.*, 3, [1], 68 – 74, (2006).

20 Wendel, M.,Clasen, R.: Investigations into the sintering of nanoscale borosilicate glass powder (in German) at the 85. Glasetchnischen Tagung der DGG, Saarbrücken (2011).

21 Tso, S.T., Pask, J.A.: Reaction of fused-silica with hydrogen gas, *J. Am. Ceram. Soc.*, 65, [9], 457 – 460, (1982).

22 Bondar, V.V., Lopatin, S.I., Stolyarova, V.L.: High-temperature thermodynamic properties of the Al_2O_3-SiO_2 system, *Inorg. Mater.*, **41**, [4], 362 – 369, (2005).

23 Snytnikov, V.N., Snytnikov, VI.N., Dubov, D.A., Zaikovskii, V.I., Ivanova, A.S., Stoyanovskii, V.O., Parmon, V.N.: Production of nanomaterials by vaporizing ceramic targets irradiated by a moderate-power continuous-wave CO_2 laser, *J. Appl. Mech. Tech. Phy.*, 48, 292 – 302, (2007).

24 Günster, J., Oelgardt, C., Heinrich, J.G., Melcher, J.: The power of light: Selforganized formation of macroscopic amounts of silica melts controlled by laser light, *Appl. Phys. Lett.*, **94**, 021114, (2009).

25 Lide, D.R. (editor): Handbook of chemistry and physics, 87thedition, CRC Press, Florida, 2006.

26 Clasen, R.: Production of very pure quartz glasses with the sintering of sub-microscopic glass particles, (in German), Faculty of mining, metallurgy and geosciences. Aachen, RWTH Aachen. Dr. habil Thesis: 464, (1989).

27 German, R.M.: Sintering theory and practice. John Wiley & Sons, Inc, New York, Chichester, Brisbane, Toronto, Singapore, 1996.

28 Scholze, H.: Glas - Natur, Struktur und Eigenschaften, (in German), Springer Verlag, Berlin, Heidelberg, New York, 1988.

29 Zarzycki, J.: Glasses and the vitreous state. Cambridge University Press, Cambridge, 1991.

30 Scholze, H.: The influence of viscosity on hot stage microscope measurements of glasses, (in German), *Ber. der DKG*, **39**, [H1], 63 – 68, (1962).

31 Barns, J.R., Hoole, A.C.F., Murrell, M.P., Welland, M.E., Broers, A.N., Bourgoin, J.P., Biebuyck, H., Johnson, M.B., Michel, B.: Characterization of electron beam induced modification of thermally grown SiO_2, *Appl. Phys. Lett.*, **67**, [11], 1538 – 1540, (1995).

32 Matsunaga, A., Kinoshita, C., Nakai, K. Tomokiyo, Y.: Radiation-induced amorphization and swelling in ceramics, *J. Nucl. Mat.*, 179 – 181, [1], 457 – 460, (1991).

33 Burden, A.P., Hutchison, J.L.: An investigation of the electron irradiation of graphite in a helium atmosphere using a modified electron microscope, *Carbon*, **35**, [4], 567 – 578, (1997).

34 Nikonorov, N.V., Sidorov, A.I., Tsekhomskii, V.A., Nashchekin, A.V., Usov, O.A., Podsvirov, O.A., Poplevkin, S.V.: Electron-beam modification of the near-surface layers of photosensitive glasses, *Tech. Phys. Lett.*, **35**, [4], 309 – 311 (2009).

35 Toth, M., Lobo, C.J., Lysaght, M.J., Vladár, A.E., Postek,M.T.: Contamination-free imaging by electron induced carbon volatilization in environmental scanning electron microscopy. *J. Appl. Phys.*, **106**, [3], 034306, (2009).

36 Vladár, A.E., Postek, M.T.: Electron beam-induced sample contamination in the SEM, *Microsc. Microanal.*, **11**, [2]. 764 – 765, (2005).